The Journal of Experimental Biology 214, 452-461

doi:10.1242/jeb.046789

## RESEARCH ARTICLE

# Scaling of mechanical power output during burst escape flight in the Corvidae

Brandon E. Jackson* and Kenneth P. Dial

Flight Laboratory, Division of Biological Sciences, The University of Montana, Missoula, MT 59812, USA

*Author for correspondence (brandon.jackson@mso.umt.edu)

Accepted 18 October 2010

**SUMMARY**

**Avian locomotor burst performance (e.g. acceleration, maneuverability) decreases with increasing body size and has significant implications for the survivorship, ecology and evolution of birds. However, the underlying mechanism of this scaling relationship has been elusive. The most cited mechanistic hypothesis posits that wingbeat frequency alone limits maximal muscular mass-specific power output. Because wingbeat frequency decreases with body size, it may explain the often-observed negative scaling of flight performance. To test this hypothesis we recorded *in vivo* muscular mechanical power from work-loop mechanics using surgically implanted sonomicrometry (measuring muscle length change) and strain gauges (measuring muscle force) in four species of Corvidae performing burst take-off and vertical escape flight. The scale relationships derived for the four species suggest that maximum muscle-mass-specific power scales slightly negatively with pectoralis muscle mass ($M_m^{-0.18}$, 95% CI: –0.42 to 0.05), but less than the scaling of wingbeat frequency ($M_m^{-0.29}$, 95% CI: –0.37 to –0.23). Mean muscle stress was independent of muscle mass ($M_m^{-0.02}$, 95% CI: –0.20 to 0.19), but total muscle strain (percent length change) scaled positively ($M_m^{0.12}$, 95% CI: 0.05 to 0.18), which is consistent with previous results from ground birds (Order Galliformes). These empirical results lend minimal support to the power-limiting hypothesis, but also suggest that muscle function changes with size to partially compensate for detrimental effects of size on power output, even within closely related species. Nevertheless, additional data for other taxa are needed to substantiate these scaling patterns.**

Supplementary material available online at http://jeb.biologists.org/cgi/content/full/214/3/452/DC1

Key words: allometry, muscle power, flight, escape.

## INTRODUCTION

Body size imposes fundamental constraints on the evolution of morphological and physiological traits (e.g. Schmidt-Nielsen, 1984). As such, most aspects of organismal locomotor performance vary with body size (e.g. cost of transport, top speed) (Schmidt-Nielsen, 1984) such that selection for a performance trait may result in selection on the corresponding morphology and body size. Burst locomotor performance (i.e. acceleration, maneuvering) is generally thought to decrease with increasing body size (e.g. Emerson, 1978; Huey and Hertz, 1984; Carrier, 1995; Domenici and Blake, 1997; Tobalske and Dial, 2000; Askew et al., 2001; Toro et al., 2003; Vanhooydonck et al., 2006; Jackson, 2009; Altshuler et al., 2010). Because burst performance is probably important for many crucial behaviors (e.g. predator–prey interactions, intraspecific competition), size may be under strong selective pressure *via* its locomotor effects (e.g. Schmidt-Nielsen, 1984; Dial et al., 2008). Identifying the morphological or physiological mechanism(s) underlying the scaling of burst performance is crucial to our understanding of the generality and importance of the scaling of locomotor performance and behavior (Dial et al., 2008).

Because of its high energetic and strict mechanical requirements, flight is the locomotor strategy most likely to suffer from detrimental scaling effects. Nevertheless, the underlying mechanism (i.e. body and limb length, muscle power output, muscle force output, etc.) should be relevant to the scaling of locomotor performance in non-flyers. The scaling of flight performance in insects with respect to flight muscle mass is a matter of debate. Indirect measurements of power output *via* maximal load lifting in a wide range of insects (49 species, 18–3180 mg) indicate positive allometry (Marden, 1987; Marden, 1994) (see also Marden and Allen, 2002; Marden, 2005). Other analyses using a modified load-lifting technique suggest negative allometry of flight performance in orchid bees (Apidae: Euglossini; 11 species, 68–817 mg) and in bumblebees (*Bombus impatiens*, 109–372 mg) (Dillon and Dudley, 2004; Buchwald and Dudley, 2010) (see also Dudley, 2000). Compared with insects, the larger size of birds makes them more tractable subjects for direct *in vivo* measurements of maximal muscle function. Maximum burst flight performance scales negatively within avian orders, approximately in proportion to body mass ($M_b$) to the –0.3 power [e.g. Columbiformes (Seveyka, 1999), Galliformes (Tobalske and Dial, 2000), Apodiformes (Altshuler et al., 2010) and Passeriformes (Jackson, 2009) (but see Askew et al., 2001)]. The traditional mechanistic hypothesis posits that mass-specific muscle power decreases with size and limits burst flight performance (hereafter the power-limiting hypothesis) (Hill, 1950; Pennycuick, 1975). Alternatively, Marden argued that mass-specific power is independent of body mass, thus performance should be limited by the ability to produce aerodynamic lift (hereafter the force-limiting hypothesis) (Marden, 1987; Marden, 1994) (see also Ellington, 1991). However, maximum mechanical muscle power has never been directly measured *in vivo* among a range of body sizes.

The power-limiting hypothesis posits that maximum flight performance is limited by the amount of power the flight muscles can produce in excess of that required for minimal flight (Pennycuick,

1975). Muscle-mass specific power output ($P_{Mm}$) is a function of wingbeat frequency ($f$), muscle stress ($\sigma$, force per unit cross sectional area), strain ($\varepsilon$, percent length change) and muscle density ($\rho$): $P_{Mm}=\sigma\varepsilon f\rho^{-1}$. The power-limiting hypothesis assumes that $\sigma$, $\varepsilon$ and $\rho$ are independent of body size as the microanatomy of vertebrate striated muscle is generally size-invariant (Hill, 1950). Wingbeat frequency scales as roughly $M_b^{-0.33}$ among extant birds (Greenewalt, 1975), leading to the prediction that $P_{Mm}$ also scales as $M_m^{-0.33}$. Because minimal mass-specific power requirements of flight vary little with size ($M_b^0$ to $M_b^{1/6}$) (Pennycuick, 1975; Ellington, 1991), the amount of excess or marginal power the muscles are capable of producing decreases with size, as does burst flight performance. Birds produce as much as 95% of the power used in flight from a single, paired muscle (m. pectoralis) (Biewener et al., 1992). The pectoralis inserts on a bony cantilever (delto-pectoral crest, DPC) conducive to biomechanical instrumentation. As such, we can reliably measure *in vivo* mechanical power output in birds (e.g. Tobalske et al., 2003) to simultaneously examine the power-limiting and force-limiting hypotheses.

Maximum burst flight performance in passerines scales as $M_b^{-0.32}$ (Jackson, 2009). To determine how muscle power output scales with body mass in those species, we surgically implanted sonomicrometry crystals and strain gauges to measure muscle strain and stress, respectively, thus directly measuring *in vivo* two critical components of muscle power (Josephson, 1985). Because the surgical techniques are difficult on smaller birds, and to control for phylogenetic effects, we chose members of the largest-bodied passerine family, Corvidae: the gray jay, *Perisoreus canadensis* L. 1766; black-billed magpie, *Pica hudsonica* Sabine 1823; American crow, *Corvus brachyrhynchos* Brehm 1822; and common raven, *C. corax* L. 1758. Performing repeatable calibrations of the strain gauges has previously been an Achilles heel for the technique (see Tobalske and Biewener, 2008), but the new technique described herein offers greater repeatability and congruence with kinematic-based aerodynamic power estimates than previous techniques.

## MATERIALS AND METHODS

Birds were trapped using remote-triggered bow nets and rocket nets baited with carrion. Birds were transported to The University of Montana's Field Research Station at Fort Missoula, MN, USA, housed in large outdoor aviaries (4×4×15 m) and provided food (e.g. raw eggs, canned dog food, wild bird seed mixes) and water *ad libitum*. Birds were housed for as few as 2 days and as long as 30 days prior to flight tests. All procedures were approved by The University of Montana Institutional Animal Care and Use Committee.

Burst take-off and vertical flight were measured in our adjustable-width experimental vertical flight chamber ('Tower of Power'; 2×2×7.6 m; Fig. 1, supplementary material Movie 1). Flight performance (the rate of change in kinematic and potential energies, or climb power, $P_{cl}$) and estimated total power output ($P_{tot}$) [a kinematic-based aerodynamic model following Wakeling and Ellington (Wakeling and Ellington, 1997) and Berg and Biewener (Berg and Biewener, 2008)] data are from Jackson (Jackson, 2009). Briefly, flights were recorded with three internally synchronized high-speed cameras (250 Hz, 1024 PCI, SA3; Photron USA, Inc., San Diego, CA, USA). Calibrated videos were digitized to determine the three-dimensional (3-D) coordinates of wing and body markers (Hedrick, 2008) (MATLAB v. 2009b, The MathWorks, Natick, MA, USA), which were used to calculate wing and body kinematics for performance measurements (analyses performed in IGOR Pro, v. 6.1, Wavemetrics, Inc., Portland, OR, USA).

Both the surgery and the added mass of cables and implants may influence flight behavior or reduce flight performance. As such, we measured whole-body performance and aerodynamic power from a single pre-surgery flight and post-surgery flights, except for the common raven. Our greatest concern with the common raven was that this notoriously intelligent species would habituate to the testing protocol. Therefore, flight performance data are presented from post-surgical flights, as the total added surgical mass (implants and full cable length) was less than 3% of $M_b$. Within 24 h of the initial

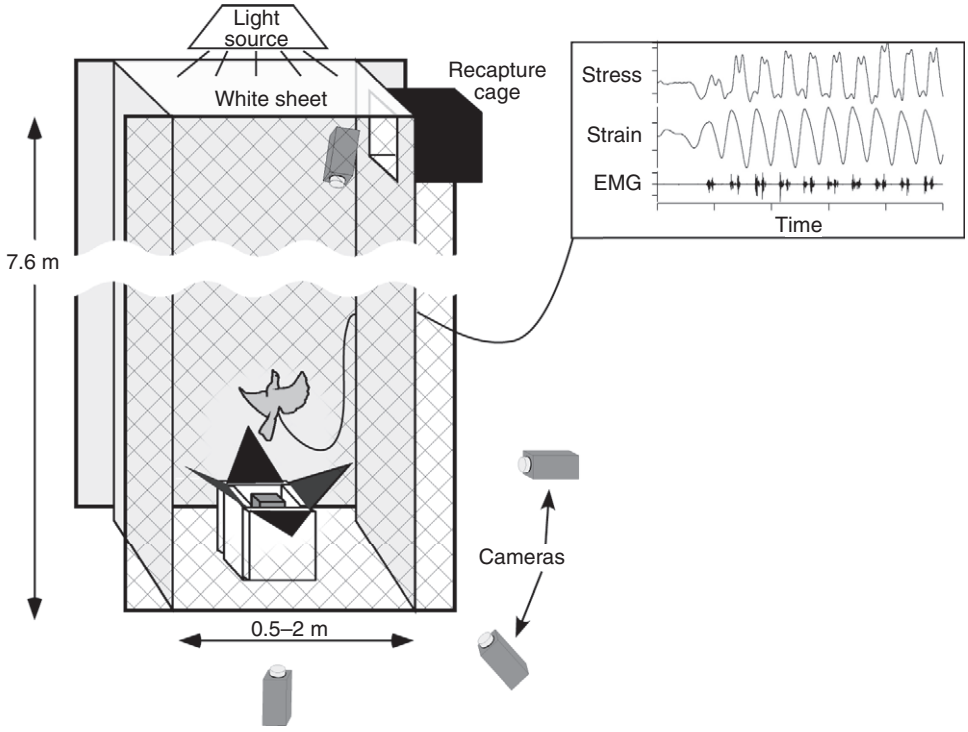


Fig. 1. Birds were filmed in our vertical flight chamber, taking off from a forceplate. Flights were induced by the sudden opening of a Plexiglas pyramid, which also contained the bird on the forceplate and directed their sight through a clear window to the white cotton sheet at the top of the tower. The width of the tower was adjusted from 0.5 to 2 m depending on the size of species being tested. Each flight was filmed with three or four high-speed cameras synchronized using a transistor-transistor logic (TTL) signal to the forceplate and *in vivo* instrument recordings. EMG, electromyography.

flight, *in vivo* recording gauges were surgically implanted; flights recorded 12–24 h after surgery. Immediately following successful recording sessions, the birds were anesthetized with inhaled isoflourane (5%) and euthanized with an overdose of sodium pentobarbital (100 mg kg$^{-1}$).

### Surgical procedures

Implant construction and surgical procedures generally followed Tobalske and Biewener (Tobalske and Biewener, 2008). All implanted gauges were soldered to a plug made of two miniature connectors (GF-6 Microtech Inc., Boothwyn, PA, USA) embedded in an epoxy platform. The gauges on each plug consisted of two single-element strain gauges (FLA-1-11, 0.5–2 mm; Tokyo Sokki Kenkyujo Co., Ltd, Tokyo, Japan), one pair of sonomicrometry crystals (1 or 2 mm, 38 or 36 AUG; Sonometrics Corp., London, Ontario, Canada), an indwelling electromyography (EMG) electrode (pair of twisted 100 µm diameter 99.9% silver wire, 1 mm inter-tip distance with 0.5 mm insulation removed; California Fine Wire Co., Grover Beach, CA, USA) and a ground wire (3 cm, 28 gauge insulated copper).

Birds were anesthetized using inhaled isofluorane (HME109, 5% to induce, 2–3% to maintain; Highland Medical Equipment, Temecula, CA, USA). Feathers were removed at each incision site (the midline between scapulae, over each DPC and over the left pectoralis). A small (1–2 cm) incision was made in the skin at each location immediately prior to implantation at that site. Implants were passed subcutaneously from the midline incision to respective implant sites. Each sonomicrometry crystal was inserted 0.5 cm deep, approximately 1.5 cm apart, into openings made along a single pectoralis fascicle near the central tendon. Each opening was closed and the crystal secured by suturing the fascia across the hole (0–6 polypropylene monofilament, Surgilene; Davis & Geck, Division of American Cyanamid Co., Danbury, CT, USA) and around the emerging wire. The EMG electrode was implanted immediately caudal to the sonomicrometry crystals. All leads were sutured to the superficial fascia with slack to control tension on the implants.

The strain gauges were implanted bilaterally on the DPC of the humerus. The implant site was cleared of muscle fibers, periosteum and fatty deposits using a bone scraper, scalpel blade and solvent (xylene or methyl-ethyl-ketone). The gauge was attached with self-catalyzing cyanoacrylate, oriented perpendicular to the long-axis of the humerus and positioned mid-distally on the DPC at the cranial edge.

The bare end of the ground wire was sutured (0–3 silk) to the intervertebral ligament at the cranial end of the synsacrum. The epoxy base of the back-plug was sutured (0–0 silk) to the intervertebral ligaments cranial to the ground wire. The skin was pulled over the epoxy base – leaving the plug exposed – sutured closed and covered with elastic surgical tape. Post-surgical birds recovered in small heated cages supplied with food and water for 12–24 h prior to flight tests.

### Acquisition and signal processing

The back plug was attached to two shielded cables with six leads each (4 m total length, 17 g m$^{-1}$ with a matching male microconnector; GM-6Cooner Wire, Chatsworth, CA, USA). The sonomicrometry signals were sent to a Tritron System 6 sonomicrometry amplifier (Triton Technology Inc., San Diego, CA, USA), the strain signals to a Measurements Group Vishay 2120A strain-gauge signal conditioner (Raleigh, NC, USA) and the EMG signals to a Grass CP511 EMG amplifier (1000× gain, 100–3000 Hz bandpass filter; West Warwick, CT, USA,). Each amplifier's output signal was recorded at 2 kHz in Axoscope (v. 10.1, Molecular Devices, Sunnyvale, CA, USA) *via* an Axon Instruments Digitata 1322 16-bit A/D converter (Union City, CA, USA).

Signal processing and analysis were performed in IGOR Pro and follow Hedrick et al. (Hedrick et al., 2003) and Tobalske and Biewener (Tobalske and Biewener, 2008). Briefly, EMG signals were filtered with a 250 Hz Butterworth high-pass filter to remove low-frequency movement artefacts, and rectified. EMG activity was defined as continuous peaks greater than two times mean baseline noise in the rectified signal. Sonomicrometry and strain gauge signals were filtered with a 50 Hz digital Butterworth low-pass filter, and corrected as in Tobalske and Dial (Tobalske and Dial, 2000) and Tobalske and Biewener (Tobalske and Biewener, 2008). Resting length ($L_{rest}$) was recorded immediately prior to each flight while the bird was enclosed on the force plate with wings folded. Muscle strain ($\varepsilon$) was calculated as $\Delta L\, L_{rest}^{-1}$, where $\Delta L$ is the difference between instantaneous fascicle length and $L_{rest}$.

### Muscle force calibration

A new technique was developed to improve the repeatability of calibrating the strain gauge recordings from the bone to muscle force (in collaboration with M. W. Bundle). Following euthanasia, the left pectoralis was exposed to verify placement of sonomicrometry crystals and EMG implantations. The wing was held in positions approximating the start, middle and end of downstroke, as observed in the high-speed video. At each position, the orientation (both proximo-distal and cranio-caudal) of the pectoral fascicles as they inserted on the ventral side of the DPC was measured using a protractor. The muscle was then dissected from the DPC and the bone was removed with the strain gauge and back-plug intact. This process was then repeated for the right pectoralis and humerus.

The articular surfaces of each end of each humerus were embedded in epoxy. A steel cable (1/64 inch diameter, 19 strands, brass-plated; Nelson Hobby Specialties, Keller, TX, USA) was adhered (Loctite® epoxy putty, Henkel Corp. Dusseldorf, Germany) to the ventral side of the DPC, immediately adjacent to the scar of the central tendon of the pectoralis. The epoxy ends were mounted in 3-D articular vices on a steel platform. The steel cable was attached to the pulley of a computer-controlled servo (CP-GV6, Gemini I/O module; Parker Compumotor, Rohnert Park, CA, USA) with a calibrated torque output on the same steel platform. The bone was positioned such that the cable had the same insertion orientation at each of the three wingstroke positions, and the motor was used to repeatedly pull (20 times) with approximate *in vivo* force while simultaneously recording motor torque and bone strain *via* the original strain gauge. To control for viscoelastic effects, motor-pull calibrations were performed at *in vivo* frequencies. An average calibration coefficient was determined for each wing position after repositioning the bone to each orientation three times. In all cases, the calibration factor declined significantly (>20%) between the start and end of downstroke positions. Given the sensitivity of calibration to the pull orientation (see also Biewener et al., 1992), we used the position-dependent calibration factors to calculate dynamic calibrations throughout the downstroke, dependent on instantaneous muscle strain. The calibration factors of the three wing positions (start, middle and end of downstroke) were associated with a muscle strain level (maximum, resting and minimum strain, respectively), and intermediate factors were determined by linear regression of calibration factor against strain level. Thus, a dynamic calibration factor, dependent on instantaneous *in vivo* muscle strain recordings, could be used to

Table 1. Morphometrics of four species of corvids

| Species | *N* | Body mass (kg) | Pectoralis mass (kg) | Fascicle length (mm) |
|---|---|---|---|---|
| Gray jay | 1 | 0.0689 | 0.0045 | 30.5 |
| Black-billed magpie | 2 | 0.1724±0.0214 | 0.0110±0.0010 | 36.7±0.7 |
| American crow | 3 | 0.3876±0.0315 | 0.0276±0.0021 | 44.5±4.0 |
| Common raven | 1 | 0.8949 | 0.0656 | 56.8 |

Pectoralis mass and fascicle length for each individual were calculated as the mean of both sides. All values are presented as species means ± s.e.m.

calibrate bone strain to muscle force accounting for changes in the orientation of fiber insertion through a downstroke. As a result, the mean (±s.d.) coefficient of variation (c.v.) among individual American crows ($N$=3) for peak stress was 15.2±8.1%. Small sample sizes ($N$=1–2 individuals) prevented similar calculations for the other species. Although this is somewhat more variable than shortening strain in the same birds (c.v.=5.3±2.2%), it is a real improvement over reported values for the older 'pull' calibration technique (e.g. c.v.=29.0±14.7%) (Tobalske et al., 2003).

### Work and power calculations

Each pectoralis muscle was carefully removed from the sternum. We determined mean fascicle length by taking 15 length

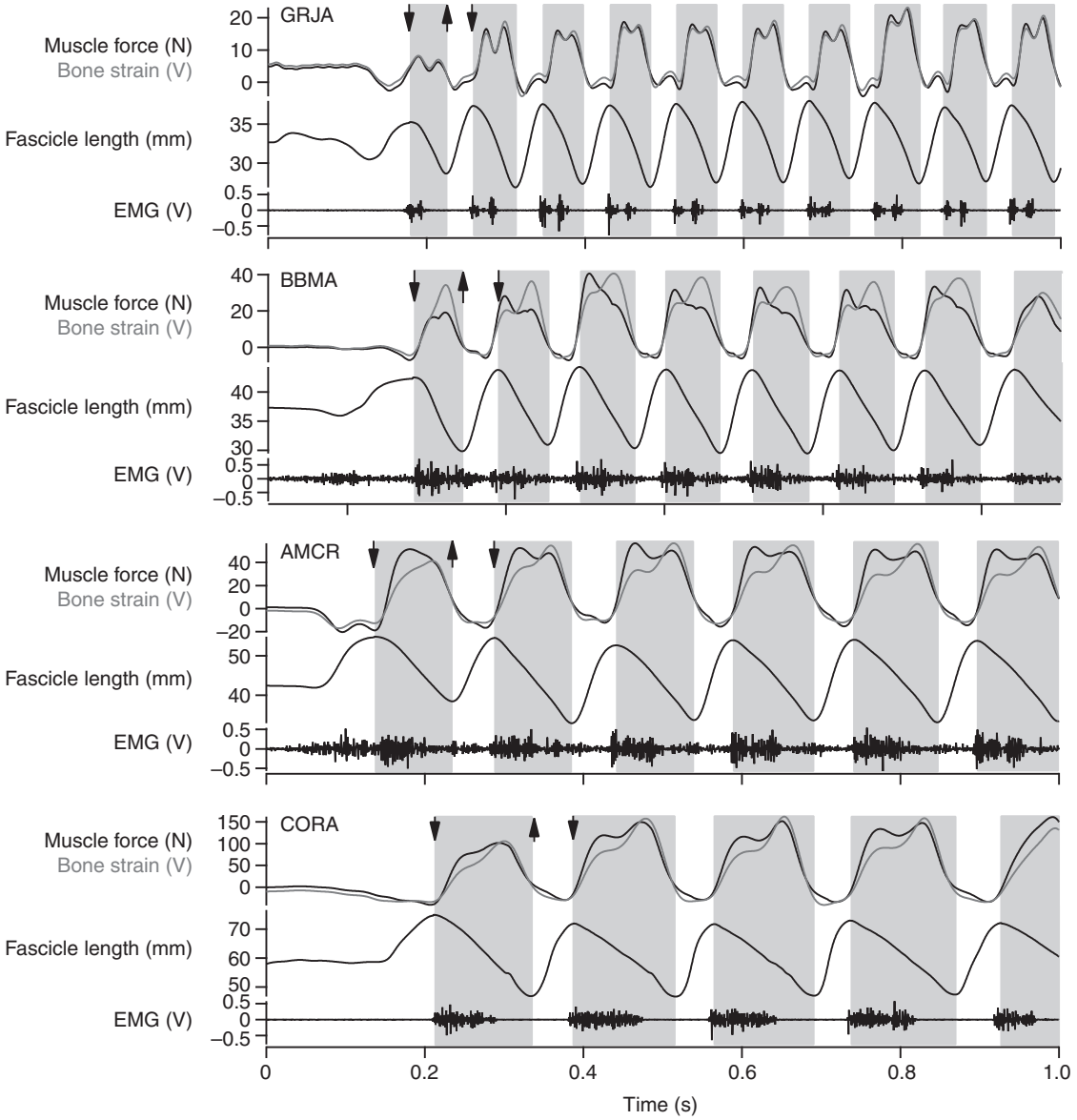


Fig. 2. Representative filtered and calibrated traces from all four species. Bone strain, as measured by the strain gauge on the humeral delto-pectoral crest (DPC) is drawn in gray to illustrate the effect of applying a dynamic calibration coefficient dependent on muscle strain. Gray shading and arrows delineate downstroke as defined by muscle fascicle shortening. AMCR, American crow; BBMA, black-billed magpie; CORA, common raven; GRJA, gray jay.

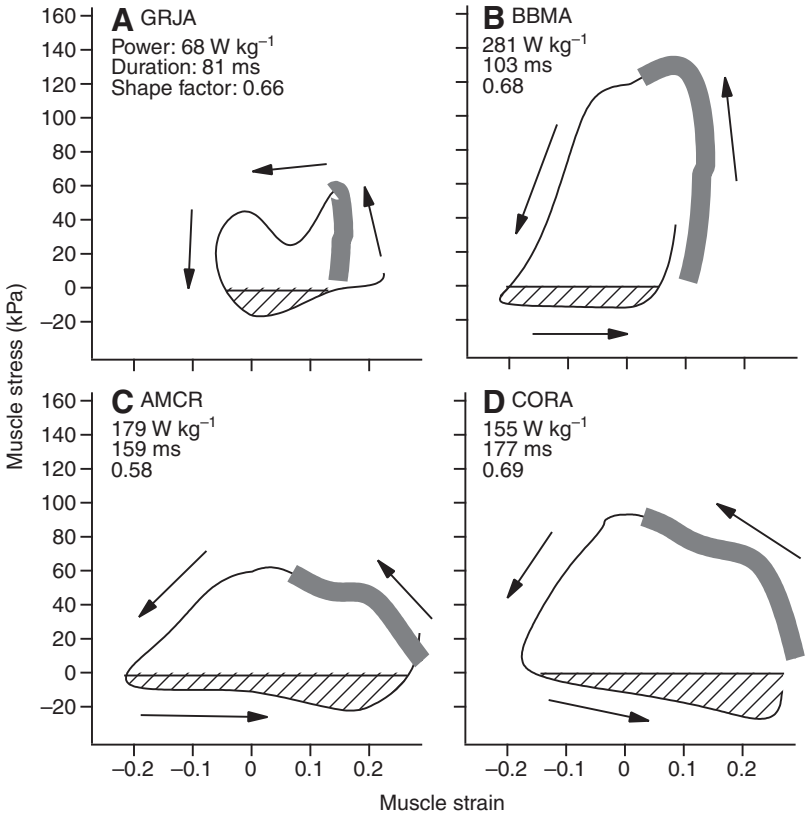


Fig. 3. Representative work loops showing the first complete wing stroke after initiation of lift-off. For GRJA, AMCR and CORA the first downstroke started before toe-off. Hashed areas are below zero muscle stress and are not included in the calculation of work or power. Thick gray lines delineate the period of EMG activity.

measurements of varying regions each of the superficial and deep surfaces of the muscle. The mass of each pectoralis was determined to 0.1 g precision using an electronic balance (Table 1).

Muscle work ($W_{mus}$) for each wingbeat was determined using the work-loop technique (Josephson, 1985; Biewener et al., 1998). The start and end of each downstroke were defined by pectoralis shortening and lengthening, respectively, as measured by sonomicrometry. The wingbeat period ($T_{wb}$) was defined as the duration of a downstroke and subsequent upstroke. The integral of muscle force against muscle length represents the positive work performed for the duration of a downstroke (i.e. during shortening). Only positive work is considered here. Muscle power ($P_{mus}$) was calculated as $W_{mus}\,T_{wb}^{-1}$. We also determined peak and average force and stress through the downstroke, fractional lengthening (muscle strain above $L_{rest}$), fractional shortening (muscle shortening below $L_{rest}$) and shape factor (the ratio of $W_{mus}$ to the area of a rectangle with dimensions of peak stress and total strain) (Hedrick et al., 2003).

### Statistical analyses

As the focus of this study was maximal muscle performance, we included only likely maximal flights in the analyses. We defined maximal flights as those where the bird took off immediately after release and flew vertically (±15 deg) for at least four full wingbeats after toe-off (the instant the bird's feet lost contact with the force plate).

In order to control for possible effects of evolutionary relationships, all data were analyzed as raw data and using models that included phylogenetic controls. We constructed a phylogeny of the four species using maximum likelihood trees based on mitochondrial genes (Bonaccorso and Peterson, 2007) in Mesquite [v. 2.71 (Maddison and Maddison, 2009), including the PDAP module (Midford et al., 2003)] using Pagel's arbitrary branch lengths (Pagel, 1992). A '.tip' file and variance–covariance matrix ('.dsc' file) were imported to Regressionv2.m (Lavin et al., 2008) for analyses in MATLAB. We used three of the models available in Regressionv2.m – ordinary least squares regression (OLS; assumes star phylogeny), phylogenetic generalized least squares (pGLS; assumes given branch lengths) and an Ornstein-Uhlenbeck transformation (RegOU) – to transform the node positions between zero (star phylogeny) and one (given branch lengths). We used species mean values to compare phylogenetic and non-phylogenetic models. Based on Akaike's information criterion (AIC), OLS always produced the best-fit models, indicating little or no phylogenetic signal (Lavin et al., 2008). Thus, for brevity, only non-phylogenetic analyses are considered.

Most variables of interest were calculated on a per-wingbeat basis. To account for the repeated measurements on individual birds, we determined regression coefficients using linear mixed-effect models (LM) with individual as a random factor (nlme module in R) (Pinheiro et al., 2009; R Development Core Team, 2009). Furthermore, as least-squares regression tends to underestimate fitted slopes, most scaling studies use some form of major axis regression (e.g. reduced major axis regression) (Tobalske and Dial, 2000). For comparison with other scaling studies, we also estimated model coefficients for species mean values using standardized major axis (SMA) regression, i.e. reduced major axis regression, SMATR module in R (see Warton and Weber, 2002; Warton et al., 2006). Measured values are presented as the means ± s.e.m. of all wingbeats from likely maximal flights. Scaling coefficients [with 95% confidence intervals (CI)] and corresponding *P*-values are presented from LM regression, unless otherwise noted.

## RESULTS

Maximal performance flights with quality implant signals were obtained from one gray jay (GRJA), two black-billed magpies (BBMA), three American crows (AMCR) and one common raven

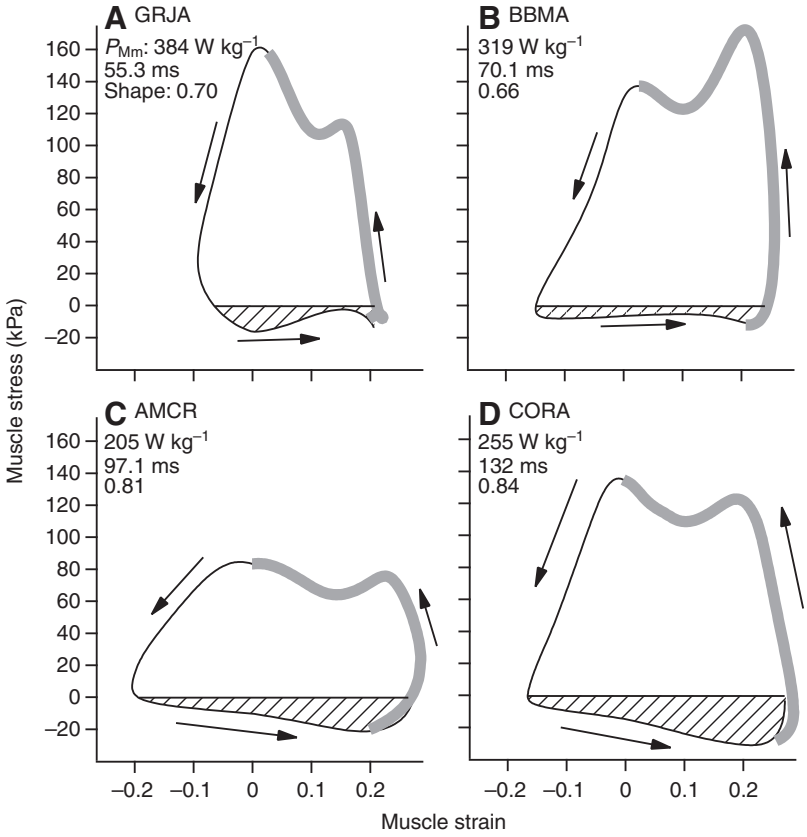


Fig. 4. Representative work loops showing the third wing stroke after initiation of lift-off. Hashed areas are below zero muscle stress and are not included in the calculation of work or power. Thick gray lines delineate the period of EMG activity.

(CORA) (Table 1). Representative implant recordings for each species are presented in Fig. 2.

Take-off styles of BBMA differed from the other species. BBMAs started their first downstroke only after their feet left the take-off surface, whereas the other species completed a partial downstroke before toe-off. All four species used a pre-lift-off counter movement. The duration and muscle strain of the first wingbeat were similar to subsequent wingbeats. However, mean and peak stresses were typically 50–70% of the mean of subsequent wingbeats, resulting in a similarly reduced mass-specific power output during the initial wingbeat (Figs 3, 4). Because the first wingbeat was unique it is not included in further analyses.

Pre-surgery flight performance after takeoff decreased with increasing body mass. The two smaller species (GRJA, BBMA) generally accelerated with every wingbeat (gaining on average 0.03 and 0.16 m s$^{-1}$ per wingbeat, respectively), but AMCR (–0.11 m s$^{-1}$) and CORA (–0.25 m s$^{-1}$) lost velocity with every wingbeat after toe-off. Body-mass-specific climb power ($P_{cl}$) showed a negative trend with $M_b^{-0.15}$ (–0.23 to –0.07, $F$=12.5, $P$=0.072; Table 2). The surgical procedure and implants significantly reduced flight performance in the GRJA (64% reduction in mean $P_{cl}$; Student's $t$-test, $t$=5.9, d.f.=2.5, $P$=0.016), but did not significantly affect BBMA (8% increase in $P_{cl}$) or AMCR (15% decrease in $P_{cl}$), with similar results for $P_{tot}$. Post-implant $P_{cl}$ was independent of $M_b$ ($F$=1.2, $P$=0.391; Table 2).

Table 2. Scaling coefficients [with 95% confidence intervals (CI)] for *in vivo* measurements from mixed-effects linear models (LM) and standardized major axis (SMA) regression, based on $\log_{10}$-transformed variables

| | | LM | | SMA | |
|---|---|---|---|---|---|
| | Independent variable | Slope (95% CI) | Slope $F$ | $P$ | Slope (95% CI) |
| Wingbeat frequency | $M_m$ | –0.29 (–0.37, –0.23) | 122.4 | <0.0001 | –0.29 (–0.45, –0.19) |
| Total strain | $M_m$ | 0.12 (0.05, 0.18) | 18.6 | 0.008 | 0.11 (0.09, 0.14) |
| Strain rate | $M_m$ | –0.22 (–0.34, –0.11) | 25.9 | 0.004 | –0.22 (–0.32, –0.16) |
| Average stress | $M_m$ | –0.01 (–0.20, 0.19) | 0.0 | 0.942 | 0.10 (0.02, 0.60) |
| Peak stress | $M_m$ | –0.09 (–0.31, 0.13) | 1.1 | 0.339 | –0.11 (–0.58, –0.02) |
| Shape factor | $M_m$ | 0.10 (0.00, 0.20) | 6.4 | 0.052 | 0.10 (0.04, 0.24) |
| $W_{Mm}$ | $M_m$ | 0.11 (–0.08, 0.30) | 2.3 | 0.192 | 0.18 (0.05, 0.67) |
| $P_{Mm}$ | $M_m$ | –0.18 (–0.42, 0.05) | 4.2 | 0.097 | –0.20 (–0.94, –0.04) |
| $P_{Mm}$ | $f$ | 0.80 (0.37, 1.23) | 13.8 | <0.0001 | 0.71 (0.18, 2.83) |
| Pre-implant $P_{cl}$ | $M_b$ | –0.15 (–0.23, –0.07)* | 12.5 | 0.072 | –0.16 (–0.43, –0.06) |
| Post-implant $P_{cl}$ | $M_b$ | 0.24 (–0.21, 0.68)* | 1.2 | 0.391 | 0.39 (0.08, 1.96) |

LMs are based on individual wingbeats, with the independent variable as a fixed effect and individual bird as a random factor ($N$=99 wingbeats, d.f.=92, 5 for all regressions). SMA analyses are based on means pooled across all individuals for a given species ($N$=4 species).

*, Ordinary linear regression based on pooled species means.

See List of abbreviations for variable definitions.

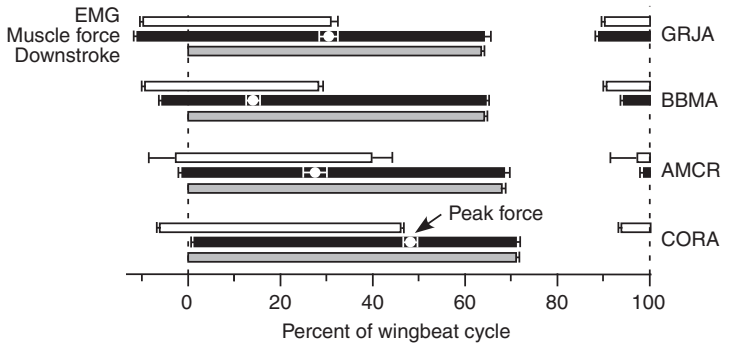


Fig. 5. Timing of EMG activity, pectoralis force production and peak force timing, and muscle shortening (i.e. downstroke) normalized as percent of the wingbeat cycle averaged for all recorded wingbeats subsequent to the first. Error bars represent ±s.e.m. of the mean normalized times of onset and offset.

Muscle stress, strain and EMG timings followed similar patterns in all species (Figs 2, 5). EMG activity and stress development started shortly before the start of muscle shortening. There were typically two stress peaks per downstroke: the first peak was larger in BBMA and AMCR, and the second peak was larger in GRJA and CORA. EMG activity continued in all species until the second stress peak (Figs 2, 4).

Pectoralis muscle mass scaled isometrically (SMA regression: $M_b^{1.05}$, 95% CI=0.97 to 1.15, $P$=0.12 for the null hypothesis that the scaling coefficient is 1.0), averaging 14.7% of $M_b$ (Table 1). Muscle-mass-specific *in vivo* power output ($P_{Mm}$) showed a negative trend with $M_m^{-0.18}$ (95% CI=–0.42 to 0.05, $F$=4.2, $P$=0.097; Fig. 6A). Wingbeat frequency scaled as $M_m^{-0.29}$ (95% CI=–0.37 to –0.23, $F$=122.4, $P$<0.0001; Table 2, Fig. 6B). Muscle-mass-specific work was independent of muscle mass ($M_m^{0.11}$, 95% CI: –0.08 to 0.30, $F$=2.3, $P$=0.192; Table 2, Fig. 6C). The GRJA produced the maximum muscle-mass-specific power produced in a single wingbeat at 471 W kg$^{-1}$ (Table 3). Mean *in vivo* muscle power accounted for 76–150% of the mean mass-specific power estimated from kinematic aerodynamic models ($P_{tot}$=109, 76, 99 and 150% for GRJA, BBMA, AMCR and CORA, respectively; Table 3).

The general shape of the work loops changed with size (Fig. 4), but both peak ($F$=1.1, $P$=0.339) and mean stresses ($F$=0.01, $P$=0.942) were independent of $M_m$ (Table 2). However, the work-loop shape factor tended to increase as $M_m^{0.10}$ (95% CI=0.00 to 0.20, $F$=6.4, $P$=0.052; Table 2). Total muscle strain also scaled with positive allometry as $M_m^{0.12}$ (95% CI=0.05 to 0.18, $F$=18.6, $P$=0.008; Table 2), ranging from 0.32 in GRJA to 0.43 in CORA (Fig. 7A, Table 3). Even though total strain increased with mass, downstroke strain rate scaled negatively as $M_m^{-0.22}$ (95% CI=–0.34 to –0.11, $F$=25.9, $P$=0.004; Fig. 7B, Table 2).

## DISCUSSION

The muscle-mass-specific power output values are suggestive of a weak negative allometry for the four species included in this study ($M_m^{-0.18}$, $P$=0.097). Yet, the implants appeared to adversely affect GRJA and not the larger species, thus the values herein for the smallest species are likely to be conservative estimates, implying that $P_{Mm}$ may scale more negatively than demonstrated. Data from species that span a wider body mass range are needed to substantiate these possible scaling patterns and to evaluate the power-limiting and force-limiting hypotheses. Contrary to the assumptions of the power-limiting hypothesis (Hill, 1950; Pennycuick, 1975), muscle strain scaled positively (as $M_m^{0.12}$); therefore, muscle power was not limited solely by wingbeat frequency.

The force-limiting hypothesis predicts that relative muscle power is independent of size (Marden, 1994). Therefore, muscle stress and/or strain would have to scale positively enough to compensate for the negative scaling of wingbeat frequency, as described for strain herein. The only other study that has examined allometric trends of *in vivo* muscle strain in burst flight also identified positive scaling of muscle strain in Galliformes ($M_b^{0.19}$), but was unable to measure muscle stress (Tobalske and Dial, 2000). Additionally, the positive scaling of shape factor (Hedrick et al., 2003) indicates that the rate and shape of force production by the pectoralis changes with body

Table 3. *In vivo* measurements and power calculations

| | Gray jay | Black-billed magpie | American crow | Common raven |
|---|---|---|---|---|
| Wingbeat frequency (Hz) | 11.6±0.0 (12.5) | 9.0±0.1 (10.3) | 6.4 ±0.1 (7.1) | 5.6±0.2 (5.8) |
| Mean $f$ (N) | 13.6±0.4 (18.4) | 30.1±0.6 (41.0) | 49.3±1.2 (60.7) | 125.1±1.2 (127.4) |
| Mean stress (kPa) | 97.7±3.1 (132.3) | 104.3±1.4 (135.3) | 69.2±6.5 (113.6) | 114.7±1.1 (116.9) |
| Peak stress (kPa) | 156.8±3.7 (220.2) | 138.5±2.3 (165.7) | 98.0±7.7 (157.7) | 137.4±1.1 (139.2) |
| Fractional lengthening ($L$ $L_{rest}^{-1}$) | 0.21±0.00 (0.26) | 0.15±0.01 (0.22) | 0.23±0.01 (0.29) | 0.27±0.01 (0.28) |
| Fractional shortening ($L$ $L_{rest}^{-1}$) | –0.12±0.00 (–0.16) | –0.20±0.01 (–0.26) | –0.14±0.01 (–0.26) | –0.17±0.00 (–0.18) |
| Shortening length (mm) | 10.0 ±0.1 (11.0) | 12.9±0.2 (14.3) | 16.5±0.8 (22.0) | 25.2±0.2 (25.6) |
| Shortening velocity ($L$ s$^{-1}$) | 6.1±0.0 (6.7) | 5.0±0.1 (5.9) | 3.7±0.1 (4.7) | 3.4±0.0 (3.5) |
| Shortening duty (% cycle) | 0.623±0.003 (0.647) | 0.624±0.005 (0.670) | 0.627±0.011 (0.684) | 0.718±0.012 (0.733) |
| $P_{Mm}$ (W kg$^{-1}$) | 350.1±10.8 (470.8) | 307.6±6.4 (355.3) | 185.1±9.3 (269.3) | 267.7±7.3 (279.6) |
| $W_{Mm}$ (J kg$^{-1}$) | 30.1±0.9 (40.7) | 34.4±0.7 (40.1) | 29.3±1.6 (44.9) | 48.0±0.3 (48.5) |
| Pre-implant $P_{tot}$ (W kg$^{-1}$) | 350±18 (410) | 395±21 (509) | 245±14 (268) | – |
| Post-implant $P_{tot}$ (W kg$^{-1}$) | 322±13 (338) | 412±12 (426) | 190±5 (196) | 271±9 (280) |
| Pre-implant $P_{cl}$ (W kg$^{-1}$) | 27.7±2.2 (31.8) | 20.9±2.2 (29.5) | 19.5±2.5 (23.9) | – |
| Post-implant $P_{cl}$ (W kg$^{-1}$) | 10.1±1.3 (11.5) | 22.6±0.1 (22.7) | 16.4±0.9 (17.3) | 18.9±3.0 (21.9) |

All values are means ± s.e.m. (maximum) for all wingbeats excluding the first; pooled within species.
See List of abbreviations for variable definitions.

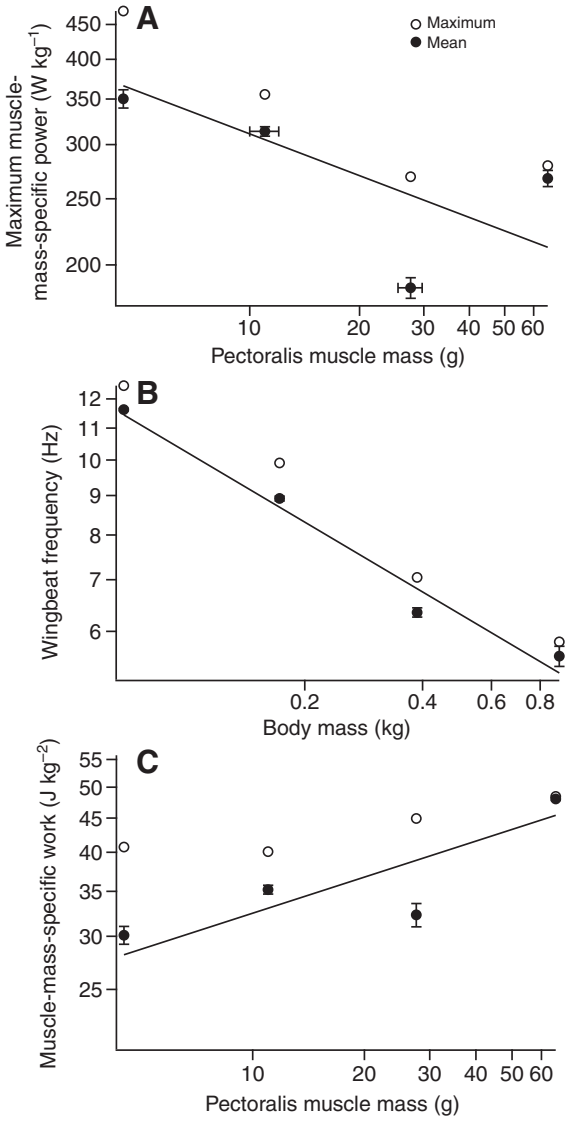


Fig. 6. (A) *In vivo* mean and maximum pectoralis mass-specific power output scaled negatively with pectoralis mass, but less negatively than (B) the scaling of wingbeat frequency. Contrary to predictions of the power-limiting hypothesis, (C) pectoralis muscle-mass specific work increased with pectoralis mass. All values are based on all recorded wingbeats subsequent to the first downstroke pooled across individuals within species. Error bars represent ±s.e.m. Scaling coefficients are shown in Table 2.

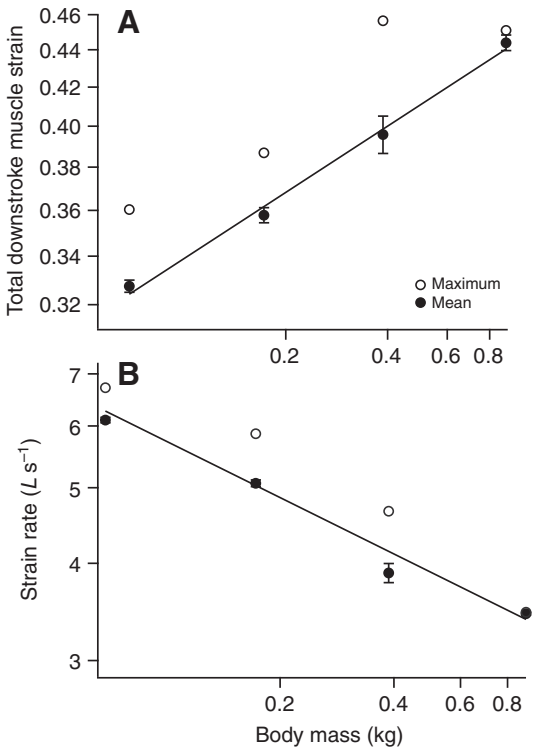


Fig. 7. (A) Total shortening strain increased with body mass, yet (B) strain rate [muscle length ($L$) s$^{-1}$] scaled negatively. All values are based on all recorded wingbeats subsequent to the first downstroke, pooled across individuals within species. Error bars represent ±s.e.m. Scaling coefficients are shown in Table 2.

size and may somewhat compensate for frequency-limited power, even though muscle stress was independent of body and muscle mass. If such compensatory mechanisms are present within a single avian family, it is likely that muscle power and flight performance across the full range of avian sizes and clades are not simply constrained by wingbeat frequency.

Previous scaling studies have struggled with two distinct challenges that were addressed in the present study: eliciting maximal performance from the animals under investigation and quantifying muscle power directly. Various authors have employed artificial load lifting in an attempt to elicit maximal flight performance from insects and birds (Marden, 1987; Marden, 1994; Chai and Millard, 1997; Altshuler et al., 2010). This technique is suitable for hummingbirds because of their innate hovering abilities and apparent comfort with the added mass (Chai et al., 1997; Altshuler et al., 2010). However, many species of birds [including those in the present study (B.E.J. and K.P.D., personal observation)] simply do not intend to fly when hindered by artificial loads unless thoroughly trained. Alternatively, marginal power has been estimated from body-mass-specific climb power ($P_{cl}$; rate change in kinetic and potential energies) during constrained vertical flight in un-weighted birds (Seveyka, 1999; Tobalske and Dial, 2000; Askew et al., 2001; Jackson, 2009) or by estimating muscle power from aerodynamic models (Askew et al., 2001; Jackson, 2009). Only Tobalske and Dial have attempted to measure *in vivo* muscle power using surgically implanted gauges, but they were stymied in recording muscle force because of the inappropriate shape of the Galliforme delto-pectoral crest as a force transducer (Tobalske and Dial, 2000). Additionally, Tobalske and Dial (Tobalske and Dial, 2000) and Askew et al. (Askew et al., 2001) used captive-bred birds, some of which had been trained or habituated to the flight tests prior to measurements. Using trained birds potentially compromises the assumption of maximal performance. Thus no previous study has successfully recorded *in vivo* muscle power during burst flights across a range of body masses.

What physiological or anatomical allometry could explain the scaling pattern of muscle strain described herein? First, avian pectoralis muscles are generally composed of two to three types of fast-twitch fibres (predominately oxidative-glycolytic fibres) that may vary in optimal contractile velocities (Rosser and George, 1986; Lundgren and Kiessling, 1988). The positive allometry of muscle strain could be explained by a positive correlation between body

mass and the proportion of more glycolytic fibres ('white' and/or 'intermediate' fibres) (Rosser and George, 1986). Tobalske (Tobalske, 1996) found such variation with body size in woodpeckers, yet the scaling of fiber composition in passerine and corvid flight muscle is unknown. Pectoralis fiber composition is only known for the second largest species included in this study, AMCR, and does not include fast-twitch glycolytic fibres as do muscles of smaller non-corvid passerines (e.g. American robin, ~75 g) (Rosser and George, 1986). Thus it appears unlikely that variation in fibre type within corvids can explain the allometry of muscle strain. Second, in small species the shorter downstroke durations may constrain the activation of flight muscle. Birds must deactivate their pectoralis during the downstroke to avoid lingering pectoralis force during the upstroke (Dial and Biewener, 1993; Biewener et al., 1998; Askew and Marsh, 2001). Many species of birds employ an asymmetrical saw-tooth cycle (i.e. >50% of cycle period spent shortening) to prolong downstroke and permit more complete activation and deactivation (Dial and Biewener, 1993; Biewener et al., 1998; Askew and Marsh, 2001; Hedrick et al., 2003; Tobalske et al., 2003). Our data suggest that large species may gain equivalent benefits as a result of having lower wingbeat frequencies and hence longer absolute shortening durations compared with smaller species. More fully activated muscles may be able to undergo greater total shortening and maintain average stresses longer, leading to changes in scaling factor.

The values of strain reported herein are similar to those from other species, whereas the values of stress are generally higher. Askew and Marsh measured *in vivo* strain and *in vitro* stress in blue quail pectoralis muscle (Askew and Marsh, 2001). Quail strain (23.4%) was similar to that of other small phasianids (19.1–22.2%) (Tobalske and Dial, 2000) but was much shorter than that of either wild turkey (35.2%) (Tobalske and Dial, 2000) or corvids (33–44%). Such high total strains have been observed in trained pigeons performing ascending flight (42%) (Tobalske and Biewener, 2008) and in cockatiels flying at very low ($1\,m\,s^{-1}$, 41%) and very high speeds ($13\,m\,s^{-1}$, 44%; minimum strain was 34% at $5\,m\,s^{-1}$) (Hedrick et al., 2003). Measurements of stress presented herein (mean peak stress in GRJA=157 kPa, max stress=220 kPa) are slightly higher than most published values for birds [blue quail *in vitro*, 131 kPa (Askew and Marsh, 2001); trained ascending pigeons, 58 kPa (Tobalske and Biewener, 2008); European starlings, 122 kPa peak isometric (Biewener et al., 1992)], as would be expected in wild birds compared with trained birds.

As a result of our relatively high stress and strain values, we found muscle power values among the highest ever measured in birds and the first *in vivo* measurements that agree with aerodynamic models. The maximum muscle-mass-specific power recorded was $471\,W\,kg^{-1}$ in GRJA (mean=$350\,W\,kg^{-1}$). Although the mean value is similar to the maximum previously reported value (*in vitro* blue quail pectoralis, $349\,W\,kg^{-1}$) (Askew and Marsh 2001), the GRJA was roughly 50% greater in mass and, therefore, may be expected to produce lower $P_{Mm}$. However, Askew and Marsh (Askew and Marsh, 2001) had difficulty with the *in vitro* preparation and suggested that their measurement may be an underestimate. Additionally and as previously mentioned, reported maximal GRJA muscle power may be an underestimate because of the effects of the implants.

Muscle power is used to induce airflow and overcome drag on the body, quantities estimated as mass-specific $P_{tot}$ from kinematic measurements. In ascending flight, previous *in vivo* measurements of $P_{Mm}$ have at best accounted for 60% of $P_{tot}$ (Tobalske and Biewener, 2008). Here we report, using the new strain gauge calibration technique, the closest agreement to date between simultaneously measured $P_{Mm}$ and $P_{tot}$ (75–150%). Several factors may explain the discrepancy between the two measures of power. First, $P_{tot}$ is an estimate for the total power output of all muscles involved in producing aerodynamically functional movements, and power from other muscles may be involved in the downstroke (e.g. sternocoracoideus, coracobrachialis) (Dial et al., 1991) but not measured by the implants. Second, some of the key assumptions of the aerodynamic models might be wrong (e.g. induced power factor, profile power costs) or altered in unknown ways by wing–wake interactions, particularly during high-power low-speed flight behaviors (Tobalske, 2007). Given the inherent difficulties with both *in vivo* measurements and kinematic estimates of total power output, a third independent technique (e.g. particle image velocimetry) may be required to further elucidate the relationship between body mass and muscle power output.

## LIST OF ABBREVIATIONS

| | |
|---|---|
| $f$ | wingbeat frequency (Hz) |
| $L$ | fascicle length (mm) |
| $L_{rest}$ | fascicle length at rest (mm) |
| $M_b$ | body mass (kg) |
| $M_m$ | pectoralis muscle mass (kg) |
| $P_{cl}$ | body-mass-specific climb power ($W\,kg^{-1}$) |
| $P_{Mm}$ | muscle-mass specific mechanical power output ($W\,kg^{-1}$) |
| $P_{mus}$ | pectoralis mechanical power output ($W\,kg^{-1}$) |
| $P_{tot}$ | body-mass-specific aerodynamic power ($W\,kg^{-1}$) |
| $T_{wb}$ | wingbeat duration (s) |
| $W_{Mm}$ | muscle-mass specific mechanical work output ($J\,kg^{-1}$) |
| $W_{mus}$ | pectoralis mechanical work output ($J\,kg^{-1}$) |
| $\varepsilon$ | muscle strain ($L\,L_{rest}^{-1}$) |
| $\rho$ | muscle density ($kg\,m^{-3}$) |
| $\sigma$ | muscle stress (kPa) |

## ACKNOWLEDGEMENTS

We thank M. Bundle for his long-term collaboration and extensive effort on the servo-motor calibration protocol, B. Tobalske and H. Davis for assistance during experimentation and comments on this manuscript, and J. Jacobs, R. Dudley, T. Martin, E. Greene, and two anonymous reviewers for comments on previous versions of the manuscript. Supported by NSF grant IBN- 0417176 to K.P.D.

## REFERENCES

**Altshuler, D. L., Dudley, R., Heredia, S. M. and McGuire, J. A.** (2010). Allometry of hummingbird lifting performance. *J. Exp. Biol.* **213**, 725-734.
**Askew, G. N. and Marsh, R. L.** (2001). The mechanical power output of the pectoralis muscle of blue-breasted quail (*Coturnix chinensis*): the *in vivo* length cycle and its implications for muscle performance. *J. Exp. Biol.* **204**, 3587-3600.
**Askew, G. N., Marsh, R. L. and Ellington, C. P.** (2001). The mechanical power output of the flight muscles of blue-breasted quail (*Coturnix chinensis*) during take-off. *J. Exp. Biol.* **204**, 3601-3619.
**Berg, A. M. and Biewener, A. A.** (2008). Kinematics and power requirements of ascending and descending flight in the pigeon (*Columba livia*). *J. Exp. Biol.* **211**, 1120-1130.
**Biewener, A. A., Dial, K. P. and Goslow, G. E.** (1992). Pectoralis muscle force and power output during flight in the starling. *J. Exp. Biol.* **164**, 1-18.
**Biewener, A., Corning, W. and Tobalske, B.** (1998). In vivo pectoralis muscle force-length behavior during level flight in pigeons (*Columba livia*). *J. Exp. Biol.* **201**, 3293-3307.
**Bonaccorso, E. and Peterson, A. T.** (2007). A multilocus phylogeny of New World jay genera. *Mol. Phylogenet. Evol.* **42**, 467-476.
**Buchwald, R. and Dudley, R.** (2010). Limits to vertical force and power production in bumblebees (Hymenoptera: *Bombus impatiens*). *J. Exp. Biol.* **213**, 426-432.
**Carrier, D. R.** (1995). Ontogeny of jumping performance in the black tailed jack rabbit (*Lepus californicus*). *J. Zool.* **98**, 309-313.
**Chai, P. and Millard, D.** (1997). Flight and size constraints: hovering performance of large hummingbirds under maximal loading. *J. Exp. Biol.* **200**, 2757-2763.
**Chai, P., Chen, J. and Dudley, R.** (1997). Transient hovering performance of hummingbirds under conditions of maximal loading. *J. Exp. Biol.* **200**, 921-929.
**Dial, K. P. and Biewener, A. A.** (1993). Pectoralis muscle force and power output during different modes of flight in pigeons (*Columba livia*). *J. Exp. Biol.* **176**, 31-54.
**Dial, K. P., Goslow, G. E., Jr and Jenkins, F., Jr** (1991). The functional anatomy of the shoulder in the European starling (*Sturnus vulgaris*). *J. Morphol.* **207**, 327-344.
**Dial, K. P., Greene, E. and Irschick, D. J.** (2008). Allometry of behavior. *Trends Ecol. Evol.* **23**, 394-401.

**Dillon, M. E. and Dudley, R.** (2004). Allometry of maximum vertical force production during hovering flight of neotropical orchid bees (Apidae: Euglossini). *J. Exp. Biol.* **207**, 417-425.
**Domenici, P. and Blake, R.** (1997). The kinematics and performance of fish fast-start swimming. *J. Exp. Biol.* **200**, 1165-1178.
**Dudley, R.** (2000). *The Biomechanics of Insect Flight: Form, Function, Evolution.* Princeton, NJ: Princeton University Press.
**Ellington, C. P.** (1991). Limitations on Animal Flight Performance. *J. Exp. Biol.* **160**, 71-91.
**Emerson, S. B.** (1978). Allometry and jumping in frogs: helping the twain to meet. *Evolution.* **32**, 551-564.
**Greenewalt, C. H.** (1975). The flight of birds: the significant dimensions, their departure from the requirements for dimensional similarity, and the effect on flight aerodynamics of that departure. *Trans. Amer. Phil. Soc.* **65**, 1-67.
**Hedrick, T. L.** (2008). Software techniques for two- and three-dimensional kinematic measurements of biological and biomimetic systems. *Bioinspir. Biomim.* **3**, 034001.
**Hedrick, T. L., Tobalske, B. W. and Biewener, A. A.** (2003). How cockatiels (*Nymphicus hollandicus*) modulate pectoralis power output across flight speeds. *J. Exp. Biol.* **206**, 1363-1378.
**Hill, A. V.** (1950). The dimensions of animals and their muscular dynamics. *Sci. Prog.* **38**, 209-230.
**Huey, R. B. and Hertz, P. E.** (1984). Effects of body size and slope on acceleration of a lizard (*Stellio Stellio*). *J. Exp. Biol.* **110**, 113-123.
**Jackson, B. E.** (2009). The Allometry of Bird Flight Performance. PhD thesis. The University of Montana, Missoula, MT, USA.
**Josephson, R. K.** (1985). Mechanical power output from striated muscle during cyclic contraction. *J. Exp. Biol.* **114**, 493-512.
**Lavin, S. R., Karasov, W. H., Ives, A. R., Middleton, K. M. and Garland, T. Jr,** (2008). Morphometrics of the avian small intestine compared with that of nonflying mammals: a phylogenetic approach. *Physiol. Biochem. Zool.* **81**, 526-550.
**Lundgren, B. O. and Kiessling, K.** (1988). Comparative aspects of fibre types, areas, and capillary supply in the pectoralis muscle of some passerine birds with differing migratory behaviour. *J. Comp. Phyiol. B* **158**, 165-173.
**Maddison, W. P. and Maddison, D. R.** (2009). Mesquite: a modular system for evolutionary analysis. Version 2.71. http://mesquiteproject.org
**Marden, J. H.** (1987). Maximum lift production during takeoff in flying animals. *J. Exp. Biol.* **130**, 235-258.
**Marden, J. H.** (1994). From damselflies to pterosaurs: how burst and sustainable flight performance scale with size. *Am. J. Physiol. Regul. Integr. Comp. Physiol.* **266**, R1077-R1084.
**Marden, J.** (2005). Scaling of maximum net force output by motors used for locomotion. *J. Exp. Biol.* **208**, 1653-1664.
**Marden, J. H. and Allen, L. R.** (2002). Molecules, muscles, and machines: universal performance characteristics of motors. *Proc. Nat. Acad. Sci. USA* **99**, 4161-4166.
**Midford, P. E., Garland, T., Jr and Maddison, W. P.** (2003). PDAP Package, Version 1.14. http://mesquiteproject.org/pdap_mesquite
**Pagel, M. D.** (1992). A method for the analysis of comparative data. *J. Theor. Biol.* **156**, 431-442.
**Pennycuick, C. J.** (1975). Mechanics of flight. *J. Avian Biol.* **5**, 1-75.
**Pinheiro, J., Bates, D., DebRoy, S., Sarkar, D. and R Development Core Team** (2009). *nlme: Linear and Nonlinear Mixed Effects Models.* R package version 3.1-93. http://www/r-project.org
**R Development Core Team** (2009). R: a language and environment for statistical computing. Vienna, Austria: R Foundation for Statistical Computing. http://www.r-project.org
**Rosser, B. W. and George, J. C.** (1986). The avian pectoralis: histochemical characterization and distribution of muscle fiber types. *Can. J. Zool.* **64**, 1174-1185.
**Schmidt-Nielsen, K.** (1984). *Scaling: Why is Size so Important.* New York: Cambridge University Press.
**Seveyka, J.** (1999). The effects of body size and morphology on the flight behavior and escape flight performance of birds. MSc thesis. The University of Montana, Missoula, MT, USA.
**Tobalske, B. W.** (1996). Scaling of muscle composition, wing morphology, and intermittent flight behavior in woodpeckers. *Auk* **113**, 151-177.
**Tobalske, B. W.** (2007). Biomechanics of bird flight. *J. Exp. Biol.* **210**, 3135-3146.
**Tobalske, B. W. and Biewener, A. A.** (2008). Contractile properties of the pigeon supracoracoideus during different modes of flight. *J. Exp. Biol.* **211**, 170-179.
**Tobalske, B. W. and Dial, K. P.** (2000). Effects of body size on take-off flight performance in the Phasianidae (Aves). *J. Exp. Biol.* **203**, 3319-3332.
**Tobalske, B. W., Hedrick, T. L., Dial, K. P. and Biewener, A. A.** (2003). Comparative power curves in bird flight. *Nature* **421**, 363-366.
**Toro, E., Herrel, A., Vanhooydonck, B. and Irschick, D. J.** (2003). A biomechanical analysis of intra- and interspecific scaling of jumping and morphology in Caribbean anolis lizards. *J. Exp. Biol.* **206**, 2641-2652.
**Vanhooydonck, B., Herrel, A., Van Damme, R. and Irschick, D. J.** (2006). The quick and the fast: the evolution of acceleration capacity in anolis lizards. *Evolution* **60**, 2137.
**Wakeling, J. M. and Ellington, C. P.** (1997). Dragonfly flight. III. Lift and power requirements. *J. Exp. Biol.* **200**, 583-600.
**Warton, D. I. and Weber, N. C.** (2002). Common slope tests for bivariate errors-in-variables models. *Biom. J.* **44**, 161-174.
**Warton, D. I., Wright, I. J., Falster, D. S. and Westoby, M.** (2006). Bivariate line-fitting methods for allometry. *Biol. Rev.* **81**, 259-291.